Altered vertebrae morphology and bone mineralization in a zebrafish model of CHARGE syndrome

Maximilian Breuer[1*]; Maximilian Rummler[2*]; Charlotte Zaouter[1]; Bettina M. Willie[2#]; Shunmoogum A. Patten[1,3#]

*, # authors contributed equally

Affiliations:

1. INRS – Centre Armand Frappier Santé Biotechnologie, 531 Boulevard des Prairies, Laval, QC, Canada, H7V 1B7
2. Research Centre, Shriners Hospital for Children-Canada, Department of Pediatric Surgery, McGill University, 1003 Decarie Blvd, Montreal, Canada H4A 0A9
3. Centre d'Excellence en Recherche sur les Maladies Orphelines - Fondation Courtois (CERMO-FC), Université du Québec à Montréal (UQAM), Montréal, QC , Canada

Key words: CHARGE syndrome, microCT, Zebrafish, late onset idiopathic scoliosis, osteogenesis

***Correspondence:** Correspondence should be addressed to
Dr. Maximilian Breuer
INRS- Centre Armand-Frappier Santé et Biotechnologie
531 Boulevard des Prairies
Laval, Quebec
H7V 1B7
Canada
Maximilian.Breuer@iaf.inrs.ca
+1 (438) 341-0445

Conflict of Interest

The authors declare no conflicts of interest

Abstract

CHARGE syndrome patients present features of idiopathic scoliosis in over 60% of cases, reduced bone mineral density and in a few cases osteopenia. While several clinical cases and studies regarding the spinal deformities in CHARGE syndrome bearing *CHD7* mutations are well-documented, the underlying mechanisms remain elusive. Here, we detect and quantitatively analyze skeletal abnormalities in adult and young *chd7*$^{-/-}$ larvae.

We show that young *chd7*$^{-/-}$ larvae present with scoliosis and kyphosis already at 9 dpf. Gene expression analysis confirmed the reduction of osteoblast markers and Pparγ targets. MicroCT analyses identified abnormal Weberian apparatus structure and vertebral body morphology in *chd7*$^{-/-}$ mutants, with highly mineralized inclusions, along with variances in bone mineral density and bone volume. Additionally, we detect a specific depletion of Col2a1a in the zebrafish vertebral cartilage, in line with a significantly reduced number of chondrocytes.

Our study is the first to elucidate the mechanisms underlying morphological changes in vertebrae of adult *chd7*$^{-/-}$ zebrafish and decreased spinal integrity. The *chd7*$^{-/-}$ zebrafish will be beneficial in future investigations of the underlying pathways of spinal deformities in CHARGE syndrome.

Introduction

Impaired bone development and spinal dysmorphisms are a major health concern in various genetic disorders. Among these, Idiopathic scoliosis is a commonly observed phenotype and the most common skeletal abnormality in children.[1] Idiopathic scoliosis is a curvature of the spine with unidentified genetic cause. However, many risk genes have been connected to the underlying mechanisms.[2] One of these related genetic disorders is the congenital multisystemic CHARGE syndrome (CS) named after the major characteristics of **C**oloboma, **H**eart defects, **A**tresea chonae, **R**etarded growth, **G**enital and **E**ar abnormalities.[3-5] Though, considering the wide variety of observed phenotypes, the list of characteristics has been continuously augmented to include craniofacial abnormalities and spinal deformations.[6-8] Along these lines, CS is closely associated with skeletal deformities such as idiopathic scoliosis, kyphosis and hemivertebrae.[9] In fact, idiopathic scoliosis is observed in a majority of CS cases, with studies showing over 60% of patients having diagnosed scoliosis at an average age of just over 6 years.[10-12] In some cases, the areal bone mineral density (aBMD) is reduced. [13]

CS is most commonly caused by a mutation in the chromodomain ATP-dependant helicase 7 (CHD7). Mutations are distributed evenly throughout the gene and the vast majority of cases are sporadic, with only very few cases of familial CS.[7, 14-16] Analysis of pathways related to CHD7 show involvement in neural crest differentiation/proliferation/migration and stem cell quiescence.[17-19] Furthermore, studies focusing on CS have identified regulatory mechanisms of CHD7 in the immune response and more strikingly in brain development.[20, 21] Most recently, CHD7 has been connected to abnormal GABAergic development resulting in an autistic-like behavior (Jamadagni et al., unpublished data). While the function of CHD7 has been extensively studied, little attention has been given to the underlying mechanisms in skeletal development.[22] Some studies have directly linked CHD7 to osteogenesis. [23, 24] Investigation in cell cultures have shown a dependency on CHD7 for successful differentiation,

more specifically to a differentiation complex with SETD1B, NLK and SMAD1 resulting in depleted osteogenesis upon depletion of CHD7 in favour of adipogenesis by regulating PPARγ target genes.[23, 24] Various models to investigate this role in vivo have been proposed. A mouse model for Chd7 deficiency, termed "looper" presents with ear ossicle malformations, but no spinal deformities.[25] However, mouse models for Chd7 deficiency have limitations, as null mutants are embryonically lethal by 10 days.[26] Yet, a recent zebrafish model has proven valuable in the modelling of *chd7* dependent CS revealing a reduction in vertebrae mineralization of young larvae.[27]

Zebrafish have become increasingly relevant in the study of fundamental bone development and bone related disorders[28-30], including scoliosis, osteoporosis, age related osteoarthritis.[31, 32] Notably, the spinal structure in zebrafish has been characterized in detail and comprises three major regions: the Weberian apparatus, a specialized structure consisting of the first four vertebrae connecting the auditory system and the swim bladder to amplify sound vibrations, the precaudal vertebrae which are connected to neural arch and spines to form the chest and, the caudal vertebrae of the tail region with neural and hemal arch.[33] Simplicity of analysis in zebrafish to investigate spinal structures has been used to understand the effects of mechanical loading on bone mineralization.[30, 34] Zebrafish have specific advantages in the analysis of skeletal development such as the closely related structure to humans, rapid bone development with first mineralization of vertebrate occurring after only 5 days post fertilization (dpf), as well as *ex utero* development and transparency of young larvae simplifying the use of *in vivo* staining and transgenic lines to allow for the analysis of early calcification in zebrafish bony structures.[35-38] Furthermore, the simplicity of high-throughput drug screening in this teleost model makes the model highly useful for investigating new drug targets and effect on skeletal development.[39, 40] These advantages have raised interest due to their high remodelling efficiency of skeletal structures including their possibility to regenerate fins, as well as the

effectiveness to reproduce spinal deformity phenotypes.[41, 42] Some of these studies in zebrafish show a close link to the Collagen Family.[43, 44] These highly conserved pathways between zebrafish and humans allow us to investigate the underlying pathomechanisms linking CHD7 to idiopathic scoliosis and other skeletal abnormalities.

We recently generated a stable *chd7*$^{-/-}$ zebrafish mutant using CRISPR/Cas9 that replicates hallmarks of CS (Jamadagni et al., unpublished data), consistent with our previous findings using a transient *chd7* morpholino knockdown model.[27] In this study we describe for the first time a detailed analysis of skeletal development in a zebrafish *chd7*$^{-/-}$ mutant model for CS. Early larvae screens reveal a delay of mineralization of vertebrae bodies linked to deficient osteoblast differentiation. Gene expression and IHC analysis reveals striking reduction in osteoblast, chondrocyte, and collagen matrix markers, particularly displaying diminished levels of Col2a1. Finally, extensive MicroCT analysis in adults show abnormal mineralization and morphological structures in precaudal and caudal vertebrae.

Results

Zebrafish chd7$^{-/-}$ *larvae show spinal deformities*

To investigate if spinal deformities are present at an early developmental stage, we screened young *chd7*$^{-/-}$ larvae at 9 dpf (n=110) for morphological abnormalities. 39% of *chd7*$^{-/-}$ larvae exhibited highly varying, scoliosis-like phenotypes at both precaudal and caudal regions of the spine (Fig. 1a). Additionally, some of these also presented with a kyphosis-like phenotype (Supplemental Fig. 1a). Even with the morphological phenotype, fish were reactive to a touch response.

chd7$^{-/-}$ *larvae have a spinal mineralization deficit that is nutrient dependent*

Given the spinal deformities in 9dpf *chd7*$^{-/-}$ larvae, we next sought to investigate the efficiency of mineralization during larval development. Calcein staining for fluorochrome labeling of

bones revealed no delay in the onset of mineralization of the first precaudal vertebrae at 6 dpf. Upon further development, at 9dpf, *chd7*$^{-/-}$ larvae showed a significant reduction in the number of calcified vertebrae (Fig. 1c). Notably, *chd7*$^{-/-}$ larvae were less efficient in complete calcification of vertebrae towards the posterior region of the spine (Fig. 1b, c).

Since calcification of the bone matrix is dependent on mineral uptake from food, we tested how the onset and development of vertebral bone structure calcification in 9 dpf *chd7*$^{-/-}$ zebrafish was dependent on nutrition accessibility. Notably, wildtype and *chd7*$^{-/-}$ larvae showed no difference in the number of mineralized vertebrae in a starvation situation between 5 dpf and 9 dpf. Expectedly, we observed significant differences when food was available from 5 dpf until 9 dpf, with *chd7*$^{-/-}$ zebrafish having a reduced number of mineralized vertebrae compared to controls. The *chd7*$^{-/-}$ larvae had the same number of mineralized vertebrae when food was available or absent (Fig. 1b, d). Starvation in zebrafish larvae between 5 dpf and 9 dpf also resulted in smaller yolks, which is to be expected, considering the high dependency on nutrition supply by the yolk. Surprisingly, we found that Weberian vertebrae, which are the first 4 vertebrae of the spinal column, were more rapidly calcified in *chd7*$^{-/-}$ larvae than in controls (Fig. 1b arrows, Fig. 1e).

We investigated if mineralization was affected in later development. Insufficient mineralization was also evident in 4-week-old juvenile zebrafish with spinal deformities. Alizarin red staining revealed decreased mineralization of caudal vertebrae, with striking deficiency toward the vertebral body (Fig. 1f).

Osteoblast differentiation is impaired in chd7$^{-/-}$ *larvae*

CHD7 has been shown to regulate osteogenesis by controlling PPARγ to promote skeletal development and regulate expression of promoting genes. To understand if the Pparγ pathway is directly involved in the observed bone mineralization deficiency and abnormal morphology in *chd7*$^{-/-}$ larvae, we tested for Pparγ target gene expression and osteoblast differentiation

marker genes at the onset of the defect at 9 dpf (Fig 1g). The key target for Pparγ, *runx2a* and *runx2b,* were significantly downregulated in *chd7*$^{-/-}$ larvae compared to controls. Further markers for osteogenesis were affected, including a significant downregulation of osteoblast markers *sp7/osterix, bglap* and *postna*. The *chd7*$^{-/-}$ larvae also had significantly lower levels of osteocyte markers and other genes regulating mineralization such as *acp5a* and *sost*, while *mgp* remained unchanged compared to control larvae. Additionally, we detected a significant upregulation of osteoclast marker *ctsk* in *chd7*$^{-/-}$ larvae.

Abnormal development of the Weberian apparatus in adult chd7$^{-/-}$ *zebrafish*

To assess the effects of *chd7* deficiency on vertebral growth and maturation, we analyzed vertebrae morphology and mass using microCT in adult zebrafish. Morphologically, adult *chd7*$^{-/-}$ zebrafish were unchanged in body length, however, appeared strikingly leaner in body stature compared to adult control zebrafish.

Since mineralization in the young larvae varied from anterior to posterior, we decided to analyze the three major structures of the zebrafish spinal column: The Weberian apparatus, precaudal and caudal vertebrae. The Weberian apparatus and its specialized structures, the supraneurals, intercalarium, tripus and parapophysis, were thinner and smaller in morphology in *chd7*$^{-/-}$ adults in comparison to controls (Fig. 2 b). We further performed a detailed analysis of volumetric bone mineral density (vBMD), bone volume (BV), total volume (TV), and bone volume fraction (BV/TV) of 1-year-old *chd7*$^{-/-}$ larvae and control zebrafish. We did not detect any significant differences in vBMD, BV or TV (Fig. 2 c-h). However, we found a significantly greater variance in TV of both intercalarium and parapophysis, as well as in BV of the parapophysis in 1-year-old *chd7*$^{-/-}$ zebrafish, as determined by F-test analysis (Supplemental Table 1). The same results were observed in 2-year-old *chd7*$^{-/-}$ compared to control zebrafish (Supplemental Table 2).

Abnormal mineralization and malformations in the body end plates of precaudal vertebrae in adult zebrafish

Vertebrae structures were analyzed by assessing key angles of the structure (Fig 3a) and mineralization features. MicroCT analysis of precaudal vertebrae identified abnormal patterns of mineralization and abnormal structures, that were especially pronounced at the arches and transverse processes in 1-year old *chd7*$^{-/-}$ and control zebrafish (Fig. 3b, c). Precaudal vertebrae showed significantly higher overall vBMD, while the distribution of mineralization between the body and arch remained unaffected (Fig. 3d, e). However, structurally, precaudal vertebrae of *chd7*$^{-/-}$ mutants show an increase of bone volume towards the body end plates of vertebrae, which in most cases show major malformations manifesting as highly mineralized inclusions (Fig. 3b, arrows). Additionally, vertebrae in 1-year-old *chd7*$^{-/-}$ zebrafish presented with a larger BV/TV compared to controls (Fig. 3g-i). Analysis of the vertebrae neural arch revealed distortion with a significantly larger rising angle, as well as a larger variance of the angles (Fig. 3f). Vertebrae showed a significantly changed body angle and significant variance of body angle and vertebrae length (Supplemental Table 3). While a depletion of vBMD in the arches and abnormal vertebrae body structure was observed in 2-year-old fish, the effects seen on total vBMD and BV were not apparent in the few samples that survived until this stage (Supplemental Fig. 2 and Supplemental Table 4). Notably, one of our *chd7*$^{-/-}$ mutants showed vertebral fusion of the analyzed precaudal vertebra and following vertebra, which was not observed in any of the controls (Supplemental Fig. 1). This further demonstrates the wide variation in severity of the bone phenotype in *chd7*$^{-/-}$ zebrafish.

Abnormal caudal vertebrae in chd7$^{-/-}$ *zebrafish vary in arch angles and reduced mineralization*

We next determined key structural features (Fig. 4a) and mineralization characteristics of caudal vertebrae. The *chd7*$^{-/-}$ zebrafish presented with warped hemal and neural arches and abnormal body structure compared to controls (Fig. 4b). Similar to precaudal vertebrae, the

growth zones of the body end plates were enlarged and showed inclusions of highly mineralized matrix (Fig. 4b). Unlike control zebrafish, *chd7*$^{-/-}$ mutants had abnormal vertebrae body structure, which usually exhibited an hourglass shape and resulting in greater variance of measured body angles (Supplemental Table 3).

In line with the neural arch screened in the precaudal vertebrae, the hemal arch in the caudal vertebrae showed significantly wider arch rising angles (Fig. 4f), while the neural arch displayed significantly greater variance (Fig. 4g) in 1-year-old *chd7*$^{-/-}$ zebrafish. In contrast to precaudal vertebrae data, the caudal vertebrae showed significantly larger variance of Total vBMD and of both arches and vertebral body vBMD (Supplemental Table 3). A significant insufficiency in mineralization of the arches compared to the vertebrae body was also measured in *chd7*$^{-/-}$ zebrafish compared to controls (Fig 4 d, e). Further analysis also revealed a significant variance in BV, TV and BV/TV in *chd7*$^{-/-}$ zebrafish compared to controls (Fig h, i).

While significantly distorted arches were still observed in 2-year old mutants, the effects on vBMD and BV were not noticed in the few surviving fish that could be screened (Supplemental Fig. 3 and Supplemental Table 4).

Col2a1 of the ECM is depleted in chd7$^{-/-}$ *zebrafish*

To obtain a more complete analysis of vertebrae integrity, we analyzed the extracellular matrix (ECM) structures of the vertebral column in 9 dpf larvae and 1-year-old *chd7*$^{-/-}$ zebrafish and controls. Hematoxylin-Eosin (HE) staining of precaudal vertebrae sections showed a significant reduction in the number of nuclei measured in the vertebral cartilage of 1-year-old *chd7*$^{-/-}$ zebrafish and controls (Fig. 5a, b). More detailed analysis using Safranin/Fast Green O staining, revealed a significant reduction in the number of chondrocytes in the vertebral cartilage in *chd7*$^{-/-}$ zebrafish in line with the HE staining (Fig. 5c, d). Additionally, both stainings indicate a hypertrophic cell morphology in *chd7* mutants. We further screened for major components of the cartilage matrix. Gene expression analysis at 9 dpf revealed a significant downregulation of

the ECM related gene *col2a1a* (Fig. 5e). Immunofluorescence showed a striking depletion of Col2a1 in the vertebral cartilage with few cells remaining, which produce a sufficient Col2a1 signal (Fig 5f). This pattern was effectively reproduced in all regions of the spine of *chd7*$^{-/-}$ zebrafish.

Discussion

Efficiency of model

CS is a multisystemic disorder likely involving a variety of underlying mechanisms that include CHD7. Therefore, different preclinical models are required to individually identify the various molecular mechanisms. Even though mouse models for CS exist, none have been reported to show the bone phenotype observed in CS patients. Our study presents a *chd7* deficient zebrafish that has a bone phenotype resembling that of CS patients, which we used to investigate skeletal development in CS. While scoliosis in CS patients has been attributed to poor muscular development, our study proposes an additional factor involving impaired early mineralization of vertebrae. In line with observations in patients, we observed spinal deformities in *chd7*$^{-/-}$ zebrafish, indicative of scoliosis.[10-12] Interestingly, our analysis reveals vertebral abnormalities are already present in young larvae of *chd7*$^{-/-}$ zebrafish. Additional clinical studies are required to investigate the onset of spinal deformities in CS patients. However, early analysis of bone density and spinal development has been suggested by CS guidelines.[45, 46] Detailed analysis may reveal less severe or early onset phenotypes. Similarly, we observed that adult *chd7*$^{-/-}$ zebrafish, which appeared without spinal deformities on visual inspection, showed signs of spinal abnormalities in microCT analysis, suggesting that mostly mild phenotypes reach this age. This is supported by the high lethality rate shown by Jamadagni et al. (unpublished), yet the underlying cause of lethality is still unclear.

Progressive skeletal disorders such as osteopenia and osteoporosis are characterized by a reduction in bone mineralization over time leading to increased fracture risk.[47] CS patients have been shown to present with significantly reduced bone mineral density.[13] Correspondingly, reduced vertebrae mineralization in *chd7*$^{-/-}$ zebrafish by 12 dpf was observed in a previous study involving morpholinos in zebrafish which had observed a reduced mineralization of vertebral structures.[27] Confirming previous data, we observed insufficient mineralization of vertebra along the posterior spinal column by 4 weeks of age. In earlier analysis of larvae at 6dpf, we were not able to detect a delay in the onset of mineralization, but already by 9 dpf we saw a significant decrease in the number of calcified vertebrae. Furthermore, mineralization appeared to be less efficient in posterior vertebrae, which could signify an impairment in ossification, since vertebrae in zebrafish undergo ossification from an anterior to posterior direction.[48] An exception from this rule is the Weberian vertebrae C1 and C2, which are ossified later in wildtypes but earlier in *chd7*$^{-/-}$ mutants.

Nutrient dependency

Our study showed that the onset of calcification was not delayed in *chd7* deficient zebrafish. However, progressing calcification was decreased already 4 days post feeding onset, even though access to food was identical in control and mutants. In contrast, differences in calcification of vertebrae in control and mutants without access to food was not significant. Previous studies have shown that feeding delay until 9 dpf does not affect future fish growth and viability and was therefore our cut-off point.[49] This data suggests that possibly an underlying mechanism involving either reduced uptake or metabolizing nutrients may play a part in the observed phenotype and this link remains to be investigated. Bone calcification and mineralization is dependent on proper nutrition and is often discussed regarding optimal bone health in humans.[50] Insufficient levels of calcium and nutritional uptake are considered an increased risk for bone injury in CS patients.[11] To optimize nutritional uptake, the

supplementation of calcium and other nutrients to counteract poor bone health has been proposed for CS patients.[51] In fact, case reports show supplementation with calcium and vitamin D significantly increased aBMD in CS patients .[52] A possible nutrient deficiency in CS, could be linked to gastrointestinal nutrient uptake difficulties in *chd7*$^{-/-}$ zebrafish[53], yet this needs to be further investigated. Thus, this possible deficiency in nutrient uptake could further hinder ossification in *chd7*$^{-/-}$ mutants. We propose using our zebrafish model of CS model to test the effect of guidelines such as calcium and nutrient supplementation, nutrient metabolism and mechanical loading in form of swim training to enhance bone strength in CS.

Loss of chd7 reduces osteogenesis in zebrafish

Osteoblast precursors commonly express differentiation markers such as *runx2* and *Osterix/sp7*.[54] Upon maturation of these osteoblasts, expression of mineralization related genes such as *bglap* (osteocalcin) are expressed. Analysis of these three genes showed that they were all significantly downregulated in *chd7*$^{-/-}$ larvae. This suggests a deficiency in mature osteoblasts, required for the mineralization of the spinal column. Misregulation or loss of theses genes, such as *osterix/sp7* has been directly linked to poor bone mineralization in zebrafish and humans.[55-57] Notably, among all osteogenesis related gene expressions significantly reduced in *chd7*$^{-/-}$ larvae, *sost*, *ctsk*, *acp5* and *col2a1* have been identified as direct regulatory targets of Chd7 by Chip-Seq.[58] Furthermore, the regulation of osteogenesis has been linked to a regulatory complex with PPARγ.[23] Cell culture experiments have proposed the role of CHD7 in osteogenesis by inhibiting PPARγ target genes by a protein complex involving CHD7, NLK and SETDB1. Upon loss of CHD7 this complex will fail to inhibit PPARγ target genes and therefore inhibit osteogenesis in preference over adipogenesis.[23] Strikingly, our qPCR results are consistent with downregulation of Pparγ target genes such as *runx2a* and *runx2b*. Furthermore, gene expression relevant for bone calcification and remodelling are misregulated

such as *sost* and *ctsk*. Thus, our study is the first to indicate the conservation of the proposed pathway shown in cell culture in an *in vivo* model.

Weberian apparatus

The Weberian apparatus is a specialized structure that connects the auditory system and the swim bladder in a complex with the first 4 vertebrae to amplify sound vibrations.[33] Our results show that key structures in the apparatus fail to efficiently form and/or mineralize. Two of these structures, the tripus and the parapophysis, are formed to connect to the swim bladder. Both are malformed in all tested *chd7*$^{-/-}$ mutants to varying degrees. This malformation may imply an inefficiency in its function concerning both the swim bladder and auditory system. Ear abnormalities are a major symptom in CS patients and functionality is affected. Furthermore, the *chd7*$^{-/-}$ mutant shows swim bladder defects (Breuer et al., unpublished) that could be additionally affecting the morphology in tripus and parapophysis or vice versa. Even though the Weberian apparatus is extremely specialized for carp and carp-like fish (Ostariophysi), it is likely that it underlies the same pathways for osteogenesis as other parts of the spine.

Abnormal vertebrae and vBMD variability

We examined volumetric bone mineral density (vBMD) and other parameters (e.g. BV, TV) in vertebral bone structures. Most strikingly, we detected large variance in density and all parameters examined, as well as some significant changes in both precaudal and caudal vertebrae. The large variance observed in *chd7*$^{-/-}$ mutants is in line with CS patients showing varying severity in spinal deformities.[12, 59] Furthermore, previous studies have shown that even minor changes in the described parameters can impact the risk for spinal deformities and fractures in disease and under treatment.[60, 61]

Another interesting feature we observed in most *chd7*$^{-/-}$ mutants, were highly mineralized inclusions, most commonly, localized towards the growth zone of the vertebrae. We did not

identify the source of these highly mineralized structures, but they could be caused by highly localized clusters of osteoblasts during vertebrae mineralization. Another possibility is the occurrence of calcified cartilage, which is more mineralized in comparison to bone. Although speculative, the occurrence of mineralized cartilage could be due to incomplete endochondral ossification, which would be in line with the reduction in *sp7/osterix* and *col2a1* expression[62, 63] Since these inclusions are highly mineralized, it seems likely that their appearance impairs the bone structurally as higher mineralized collagen is stiffer, yet less tough.[64] It will be of interest to see if future studies can take a closer look at these previously unidentified features. While these minor defects could be involved in the structural integrity of the spine in CS patients, these minor features may be missed during dual-energy x-ray absorptiometry (DEXA) screens of CS patients when assessing aBMD.

Analysis revealed a decreased mineralization in the caudal vertebral arches of the mutant fish. This likely reduces the mechanical competence of these vertebrae in comparison to healthy vertebrae. A compromised mechanical competence alongside low BMD also increases fracture risk and can be an underlying cause of scoliosis.[65-67] Unfortunately, natural history BMD data of CS patients throughout early development is not available, to the best of our knowledge. However, aBMD analysis of patients with idiopathic scoliosis in CS via DEXA scans has been studied and shows significant reduction in some cases.[13, 68] In general, there is an increased fracture risk and incidence of scoliosis corresponding to decreased BMD, such as in osteopenia and osteoporosis.[47, 66] In line with this reduced mineralization an increased fracture and injury risk has been reported for CS patients.[13] Accordingly, proper observation and focus on early DEXA analysis is considered for CS guidelines.[45, 46]

Our analysis throughout development of *chd7*$^{-/-}$ deficient zebrafish suggests that only mild phenotypes survive onto later stages with severity decreasing as age progresses. However, the high lethality in both patients and our model is connected to a multisystemic phenotype in which

one mechanism is unlikely to be exclusive underlying cause for this characteristic. The link between Chd7 and severe spinal and vertebrae abnormalities, including kyphosis, fused vertebrae and hemivertebrae has been observed in our samples.[7, 9]

Collagen and chondrocyte depletion as additional risk factor

Our data in *chd7* deficient zebrafish indicate that reduced vBMD may not be the only underlying risk factor for idiopathic scoliosis in CS patients. Spinal integrity may be weakened by a decrease in chondrocyte marker *col2a1* expression in the vertebral cartilage of *chd7* deficient zebrafish. Col2a1 is required in the ECM of various cell types including osteoblasts, chondrocytes, external ligament connective tissue cells, as well as notochord basal cells and expressed in the corresponding tissues.[69, 70] Each cell type is required for proper integrity and could likely contribute to spinal injuries and malformations. Furthermore, *col2a1a* expression is observed throughout ossification of the notochord.[71] Reduction in this collagen matrix in the notochord can affect proper calcification. *Col2a1a* is expressed in osteoblasts and chondrocytes of teleosts and regulated by *sox9*, which in turn is known to be regulated by *Chd7*.[72-74] The hypertrophic morphology of the chondrocytes seen in our study may indicate signs of a weakened matrix, as well as altered matrix composition and may contribute to an increased risk in osteoporosis.[75, 76] How this regulatory defect may influence other cartilage/skeletal regions such as the craniofacial cartilage remains to be investigated.

In summary, our study is the first to identify skeletal abnormalities linked to *chd7* deficiency. These abnormalities include morphological changes in vertebrae, reduced bone mineralization, impaired osteoblast activity, highly mineralized inclusions and Col2a1 deficiency in the *chd7*$^{-/-}$ zebrafish model organism. The use of this preclinical model will allow for future studies to further understand the underlying mechanisms of spinal deformities in CS.

Materials and Methods

Zebrafish husbandry

Wildtype (Cntrl) and mutant (*chd7*$^{-/-}$) zebrafish were kept at 28°C in a 12h/12h dark/light cycle and maintained in accordance with Westerfield et al.[77]. All zebrafish in this study were fed a steady diet of Skretting®GemmaMicro starting at 5dpf. Embryos were raised at 28.5°C and staged as previously described by Kimmel et al.[78] All experiments were performed in with the guidelines of the Canadian Council for Animal Care and the local ethics committee.

Skeletal stainings and analysis of larvae

Calcein staining was done as described[38]. In short, zebrafish larvae at 9dpf were exposed to calcein (2g/L) (Sigma-Aldrich) in water for 10 minutes. Larvae were then washed at least 3 times in fish water for 10 minutes to remove excess calcein. Larvae were then anesthetized using tricaine before being imaged using an AxioZoom V16 (Zeiss). For nutrition dependency tests, larvae were either deprived of food until 9 dpf or fed a regular Skretting®GemmaMicro diet starting at 5 dpf.

Alizarin Red was performed as previously shown[79]. In brief, larvae were fixed for 2 hours with 2% PFA. The PFA was then removed by washes in PBS 3x10 minutes and then placed in 25% glycerol/0.1%KOH. Finally, larvae were stained with 0,05% Alizarin Red (Sigma-Aldrich) in H_2O for 30 minutes and stored in 50% glycerol in 0.1%KOH.

MicroCT Imaging

Adult zebrafish were euthanized using tricaine (MS-222, Sigma-Aldrich). Tissue was fixed in 4% PFA prior to microCT analysis. Ex vivo microCT at an isotropic voxel size of 10.6 µm (SkyScan1276, Bruker, Kontich, Belgium) was performed to assess differences in bone mass, mineral density, and microstructure. The following scanning parameters were used: peak voltage of 55 kVp, Aluminum 0.25 mm filter, source current of 200 µA, 0.3° rotational steps

for full 360° with no frame averaging. Images were reconstructed using standard reconstruction algorithms provided with the microCT. Spinal deformities of controls and mutants were analyzed of 1-year (n=8 for Cntrl and n=8 *chd7*$^{-/-}$) and 2-year-old (n=5 for Cntrl and n=5 *chd7*$^{-/-}$) zebrafish.

Analysis and bone density/volume/angles

From the reconstructed microCT images of the whole spine, the Weberian apparatus, as well as vertebrae 7 (abdominal) and 20 (caudal) were segmented. Further, the intercalarium, the tripus as well as the parapophysis were segmented from the Weberian apparatus. For the vertebrae, the neural as well as the hemal arch were segmented from the vertebral body. To differentiate between bone and background, a density-based threshold of 0.41 gHA/cm^3 determined by Otsu's method[80] was used. For each segmented bone in the Weberian apparatus outcomes included: bone volume BV (mm^3), tissue volume TV (mm^3), bone volume fraction BV/TV (mm^3/mm^3) and volumetric bone mineral density vBMD (gHA/cm^3). For abdominal and caudal vertebrae the outcomes included: bone volume BV, tissue volume TV, bone volume fraction BV/TV, total bone mineral density T.vBMD, vertebral body vBMD VB.BMD, vertebral arch vBMD VA.BMD, as well as arch-body angle, body angle, arch opening angle and rising angles (see Fig.2a and 3a). For caudal vertebrae, the angle outcomes were calculated for hemal as well as neural arches.

qRT-PCR

Total RNA was isolated from 9 dpf old zebrafish larvae using TriReagent. 1µg of RNA was used for cDNA synthesis using cDNA vilo kit. qRT-PCR was performed with SYBR Green mix (BIORAD) with a Lightcycler96® (Roche). Gene expression was analyzed relative to the housekeeping gene elf1α. Primers used for *runx2a, runx2b, sost, bglap, sp7/osterix, mgp, postna, acp5a, ctsk, col2a1 and mgp* are shown in supplementals Table 5.

Spinal sections/Stainings/Immunohistochemistry

The zebrafish were euthanized in tricaine (MS-222, Sigma-Aldrich) and fixed for 3 days in 4% paraformaldehyde at 4°C, after the abdomen was opened to ensure proper fixation. The spinal cords were dissected and decalcified with EDTA 10 % for 3 days under agitation at RT. After fixation and decalcification, the zebrafish were embedded in paraffin. Longitudinal sections (5µm) were obtained and were deparaffinized in xylene and were rehydrated in a graded series of ethanol. The slides were stained with hematoxylin (STATLAB Medical Products, LLC) for 4 min, and washed with alcohol-acid, and were rinsed with tap water. In the blueing step, the slides were soaked in saturated lithium carbonate solution for 10 sec, and then rinsed with tap water. Finally, staining was performed with eosin Y (STATLAB Medical Products, LLC) for 2 min and mounted with Permount™ mounting medium.

For Safranin O/Fast green, after dehydration, the slides were stained with Weigert's hematoxylin (Sigma-Aldrich) for 4 min, wash under tap water, immersed in alcohol–acid for 5 sec, then washed under water. The slides were stained with Fast green 0.02 % for 2 min, washed with acetic water 1% for 20 sec, then stained directly in safranin 0.01 % for 5 min and mounted with Permount™ mounting medium. Images were taken using an AxioZoom V16 (Zeiss) and area and number of nuclei were determined using ImageJ.

Immunofluorescence for Col2a1 was performed as previously shown[69]. In short, Epitope demasking was performed by digestion with Proteinase K (20µg/ml). Tissue was blocked with NGS and samples treated with primary antibody for Col2a1 (1 in 10; Developmental studies hybridoma bank) and secondary antibody Goat-anti-Mouse Alexafluor 488 (1 in 300). Counter stain was done using DAPI-mounting medium. Images were taken using a LSM780 (Zeiss).

Statistics

Statistical analysis was carried out using Prism-GraphPad® (GraphPad, San Diego, CA, USA). qPCR data and nuclei quantification were tested with student's t-test. Calcification analysis in larvae was performed with one-way ANOVA and post-hoc Tukey Test. MiroCT data of Control vs *chd7*$^{-/-}$ mutants was analyzed using student's t-test with Welch's correction and Variance determined by F-test analysis. Significance was determined at *<0,05; **<0,01 and ***<0,001

Acknowledgements

The authors would like to thank Beatrice Steyn for experimental support and Mark Lepik for graphic design. SP is supported by the Natural Science and Engineering Research Council (NSERC), Canadian Institutes of Health Research (CIHR), an ALS Canada-Brain Canada Career Transition Award and a FRQS Junior 1 research scholar. BMW is supported by FRQS Programme de bourses de chercheur. MR is supported by FRQS Programme de bourses de chercheur. We also thank Shriners Hospital for Children and the CIHR (165939) for financial support.

Author roles

MB, MR, BMW and SP designed the study. MB, MR and CZ performed the experiments. MB and MR drafted the manuscript. MB, MR, CZ, BMW, SP edited the mansucript.

References

1. Wise CA, Gao X, Shoemaker S, Gordon D, Herring JA. Understanding genetic factors in idiopathic scoliosis, a complex disease of childhood. Curr Genomics. 2008;9(1):51-9.
2. Grauers A, Einarsdottir E, Gerdhem P. Genetics and pathogenesis of idiopathic scoliosis. Scoliosis Spinal Disord. 2016;11:45.
3. Hall BD. Choanal atresia and associated multiple anomalies. J Pediatr. 1979;95(3):395-8.
4. Hittner HM, Hirsch NJ, Kreh GM, Rudolph AJ. Colobomatous microphthalmia, heart disease, hearing loss, and mental retardation--a syndrome. J Pediatr Ophthalmol Strabismus. 1979;16(2):122-8.

5. Pagon RA, Graham JM, Jr., Zonana J, Yong SL. Coloboma, congenital heart disease, and choanal atresia with multiple anomalies: CHARGE association. J Pediatr. 1981;99(2):223-7.
6. Blake KD, Salem-Hartshorne N, Daoud MA, Gradstein J. Adolescent and adult issues in CHARGE syndrome. Clin Pediatr (Phila). 2005;44(2):151-9.
7. Jongmans MC, Admiraal RJ, van der Donk KP, Vissers LE, Baas AF, Kapusta L, et al. CHARGE syndrome: the phenotypic spectrum of mutations in the CHD7 gene. J Med Genet. 2006;43(4):306-14.
8. Verloes A. Updated diagnostic criteria for CHARGE syndrome: a proposal. Am J Med Genet A. 2005;133A(3):306-8.
9. Sanlaville D, Verloes A. CHARGE syndrome: an update. Eur J Hum Genet. 2007;15(4):389-99.
10. Doyle C, Blake K. Scoliosis in CHARGE: a prospective survey and two case reports. Am J Med Genet A. 2005;133A(3):340-3.
11. Forward KE, Cummings EA, Blake KD. Risk factors for poor bone health in adolescents and adults with CHARGE syndrome. Am J Med Genet A. 2007;143A(8):839-45.
12. Gao X, Gordon D, Zhang D, Browne R, Helms C, Gillum J, et al. CHD7 gene polymorphisms are associated with susceptibility to idiopathic scoliosis. Am J Hum Genet. 2007;80(5):957-65.
13. Kumaran A, Kirk J. Endocrine manifestations of CHARGE syndrome. Endocrine Abstracts. 2013;33:P80.
14. Lalani SR, Safiullah AM, Fernbach SD, Harutyunyan KG, Thaller C, Peterson LE, et al. Spectrum of CHD7 mutations in 110 individuals with CHARGE syndrome and genotype-phenotype correlation. Am J Hum Genet. 2006;78(2):303-14.
15. Mitchell JA, Giangiacomo J, Hefner MA, Thelin JW, Pickens JM. Dominant CHARGE association. Ophthalmic Paediatr Genet. 1985;6(1-2):271-6.
16. Delahaye A, Sznajer Y, Lyonnet S, Elmaleh-Berges M, Delpierre I, Audollent S, et al. Familial CHARGE syndrome because of CHD7 mutation: clinical intra- and interfamilial variability. Clin Genet. 2007;72(2):112-21.
17. Jones KM, Saric N, Russell JP, Andoniadou CL, Scambler PJ, Basson MA. CHD7 maintains neural stem cell quiescence and prevents premature stem cell depletion in the adult hippocampus. Stem Cells. 2015;33(1):196-210.
18. Ohta S, Yaguchi T, Okuno H, Chneiweiss H, Kawakami Y, Okano H. CHD7 promotes proliferation of neural stem cells mediated by MIF. Mol Brain. 2016;9(1):96.
19. Okuno H, Renault Mihara F, Ohta S, Fukuda K, Kurosawa K, Akamatsu W, et al. CHARGE syndrome modeling using patient-iPSCs reveals defective migration of neural crest cells harboring CHD7 mutations. Elife. 2017;6.
20. Writzl K, Cale CM, Pierce CM, Wilson LC, Hennekam RC. Immunological abnormalities in CHARGE syndrome. Eur J Med Genet. 2007;50(5):338-45.
21. Feng W, Shao C, Liu HK. Versatile Roles of the Chromatin Remodeler CHD7 during Brain Development and Disease. Front Mol Neurosci. 2017;10:309.
22. Janssen N, Bergman JE, Swertz MA, Tranebjaerg L, Lodahl M, Schoots J, et al. Mutation update on the CHD7 gene involved in CHARGE syndrome. Hum Mutat. 2012;33(8):1149-60.
23. Takada I, Kouzmenko AP, Kato S. Wnt and PPARgamma signaling in osteoblastogenesis and adipogenesis. Nat Rev Rheumatol. 2009;5(8):442-7.
24. Chen Y, Wang M, Chen D, Wang J, Kang N. Chromatin remodeling enzyme CHD7 is necessary for osteogenesis of human mesenchymal stem cells. Biochem Biophys Res Commun. 2016;478(4):1588-93.

25. Ogier JM, Carpinelli MR, Arhatari BD, Symons RC, Kile BT, Burt RA. CHD7 deficiency in "Looper", a new mouse model of CHARGE syndrome, results in ossicle malformation, otosclerosis and hearing impairment. PLoS One. 2014;9(5):e97559.
26. Hurd EA, Capers PL, Blauwkamp MN, Adams ME, Raphael Y, Poucher HK, et al. Loss of Chd7 function in gene-trapped reporter mice is embryonic lethal and associated with severe defects in multiple developing tissues. Mamm Genome. 2007;18(2):94-104.
27. Patten SA, Jacobs-McDaniels NL, Zaouter C, Drapeau P, Albertson RC, Moldovan F. Role of Chd7 in zebrafish: a model for CHARGE syndrome. PLoS One. 2012;7(2):e31650.
28. Busse B, Galloway JL, Gray RS, Harris MP, Kwon RY. Zebrafish: An Emerging Model for Orthopedic Research. J Orthop Res. 2020;38(5):925-36.
29. Carnovali M, Banfi G, Mariotti M. Zebrafish Models of Human Skeletal Disorders: Embryo and Adult Swimming Together. Biomed Res Int. 2019;2019:1253710.
30. Ofer L, Dean MN, Zaslansky P, Kult S, Shwartz Y, Zaretsky J, et al. A novel nonosteocytic regulatory mechanism of bone modeling. PLoS Biol. 2019;17(2):e3000140.
31. Hayes AJ, Reynolds S, Nowell MA, Meakin LB, Habicher J, Ledin J, et al. Spinal deformity in aged zebrafish is accompanied by degenerative changes to their vertebrae that resemble osteoarthritis. PLoS One. 2013;8(9):e75787.
32. Bergen DJM, Kague E, Hammond CL. Zebrafish as an Emerging Model for Osteoporosis: A Primary Testing Platform for Screening New Osteo-Active Compounds. Front Endocrinol (Lausanne). 2019;10:6.
33. Dahdul WM, Lundberg JG, Midford PE, Balhoff JP, Lapp H, Vision TJ, et al. The teleost anatomy ontology: anatomical representation for the genomics age. Syst Biol. 2010;59(4):369-83.
34. Suniaga S, Rolvien T, Vom Scheidt A, Fiedler IAK, Bale HA, Huysseune A, et al. Increased mechanical loading through controlled swimming exercise induces bone formation and mineralization in adult zebrafish. Sci Rep. 2018;8(1):3646.
35. Haga Y, Dominique VJ, 3rd, Du SJ. Analyzing notochord segmentation and intervertebral disc formation using the twhh:gfp transgenic zebrafish model. Transgenic Res. 2009;18(5):669-83.
36. Morin-Kensicki EM, Melancon E, Eisen JS. Segmental relationship between somites and vertebral column in zebrafish. Development. 2002;129(16):3851-60.
37. Spoorendonk KM, Hammond CL, Huitema LFA, Vanoevelen J, Schulte-Merker S. Zebrafish as a unique model system in bone research: the power of genetics and in vivo imaging. 2010;26(2):219-24.
38. Xi Y, Chen D, Sun L, Li Y, Li L. Characterization of zebrafish mutants with defects in bone calcification during development. Biochem Biophys Res Commun. 2013;440(1):132-6.
39. MacRae CA, Peterson RT. Zebrafish as tools for drug discovery. Nature reviews Drug discovery. 2015;14(10):721-31.
40. Fleming A, Sato M, Goldsmith P. High-throughput in vivo screening for bone anabolic compounds with zebrafish. J Biomol Screen. 2005;10(8):823-31.
41. Boswell CW, Ciruna B. Understanding Idiopathic Scoliosis: A New Zebrafish School of Thought. Trends Genet. 2017;33(3):183-96.
42. Guo L, Ikegawa S, Shukunami C. Emergence of Zebrafish as a Model System for Understanding Human Scoliosis. In: Hirata H, Iida A, editors. Zebrafish, Medaka, and Other Small Fishes: New Model Animals in Biology, Medicine, and Beyond. Singapore: Springer Singapore; 2018. p. 217-34.
43. Gray RS, Wilm TP, Smith J, Bagnat M, Dale RM, Topczewski J, et al. Loss of col8a1a function during zebrafish embryogenesis results in congenital vertebral malformations. Dev Biol. 2014;386(1):72-85.

44. Gistelinck C, Kwon RY, Malfait F, Symoens S, Harris MP, Henke K, et al. Zebrafish type I collagen mutants faithfully recapitulate human type I collagenopathies. Proc Natl Acad Sci U S A. 2018;115(34):E8037-E46.
45. de Geus CM, Free RH, Verbist BM, Sival DA, Blake KD, Meiners LC, et al. Guidelines in CHARGE syndrome and the missing link: Cranial imaging. Am J Med Genet C Semin Med Genet. 2017;175(4):450-64.
46. Trider CL, Arra-Robar A, van Ravenswaaij-Arts C, Blake K. Developing a CHARGE syndrome checklist: Health supervision across the lifespan (from head to toe). Am J Med Genet A. 2017;173(3):684-91.
47. Aspray TJ, Hill TR. Osteoporosis and the Ageing Skeleton. Subcell Biochem. 2019;91:453-76.
48. Bensimon-Brito A, Cardeira J, Cancela ML, Huysseune A, Witten PE. Distinct patterns of notochord mineralization in zebrafish coincide with the localization of Osteocalcin isoform 1 during early vertebral centra formation. BMC Dev Biol. 2012;12:28.
49. Hernandez RE, Galitan L, Cameron J, Goodwin N, Ramakrishnan L. Delay of Initial Feeding of Zebrafish Larvae Until 8 Days Postfertilization Has No Impact on Survival or Growth Through the Juvenile Stage. Zebrafish. 2018;15(5):515-8.
50. O'Keefe JH, Bergman N, Carrera-Bastos P, Fontes-Villalba M, DiNicolantonio JJ, Cordain L. Nutritional strategies for skeletal and cardiovascular health: hard bones, soft arteries, rather than vice versa. Open Heart. 2016;3(1):e000325.
51. Blake KD, Hudson AS. Gastrointestinal and feeding difficulties in CHARGE syndrome: A review from head-to-toe. Am J Med Genet C Semin Med Genet. 2017;175(4):496-506.
52. Foppiani L, Maffe A, Forzano F. CHARGE syndrome as unusual cause of hypogonadism: endocrine and molecular evaluation. Andrologia. 2010;42(5):326-30.
53. Cloney K, Steele SL, Stoyek MR, Croll RP, Smith FM, Prykhozhij SV, et al. Etiology and functional validation of gastrointestinal motility dysfunction in a zebrafish model of CHARGE syndrome. FEBS J. 2018;285(11):2125-40.
54. Ortuno MJ, Susperregui AR, Artigas N, Rosa JL, Ventura F. Osterix induces Col1a1 gene expression through binding to Sp1 sites in the bone enhancer and proximal promoter regions. Bone. 2013;52(2):548-56.
55. Kague E, Roy P, Asselin G, Hu G, Simonet J, Stanley A, et al. Osterix/Sp7 limits cranial bone initiation sites and is required for formation of sutures. Dev Biol. 2016;413(2):160-72.
56. Lapunzina P, Aglan M, Temtamy S, Caparros-Martin JA, Valencia M, Leton R, et al. Identification of a frameshift mutation in Osterix in a patient with recessive osteogenesis imperfecta. Am J Hum Genet. 2010;87(1):110-4.
57. Niu P, Zhong Z, Wang M, Huang G, Xu S, Hou Y, et al. Zinc finger transcription factor Sp7/Osterix acts on bone formation and regulates col10a1a expression in zebrafish. Science Bulletin. 2017;62(3):174-84.
58. Rouillard AD, Gundersen GW, Fernandez NF, Wang Z, Monteiro CD, McDermott MG, et al. The harmonizome: a collection of processed datasets gathered to serve and mine knowledge about genes and proteins. Database (Oxford). 2016;2016.
59. Tilley MK, Justice CM, Swindle K, Marosy B, Wilson AF, Miller NH. CHD7 gene polymorphisms and familial idiopathic scoliosis. Spine (Phila Pa 1976). 2013;38(22):E1432-6.
60. Faulkner KG. Bone matters: are density increases necessary to reduce fracture risk? J Bone Miner Res. 2000;15(2):183-7.
61. Li XF, Li H, Liu ZD, Dai LY. Low bone mineral status in adolescent idiopathic scoliosis. Eur Spine J. 2008;17(11):1431-40.
62. Oh JH, Park SY, de Crombrugghe B, Kim JE. Chondrocyte-specific ablation of Osterix leads to impaired endochondral ossification. Biochem Biophys Res Commun. 2012;418(4):634-40.

621 63. Weigele J, Franz-Odendaal TA. Functional bone histology of zebrafish reveals two
622 types of endochondral ossification, different types of osteoblast clusters and a new bone type.
623 J Anat. 2016;229(1):92-103.
624 64. Currey JD. Bones: Structure and Mechanics: Princeton University Press; 2006.
625 65. Zimmermann EA, Busse B, Ritchie RO. The fracture mechanics of human bone:
626 influence of disease and treatment. Bonekey Rep. 2015;4:743.
627 66. Sarioglu O, Gezer S, Sarioglu FC, Koremezli N, Kara T, Akcali O, et al. Evaluation of
628 vertebral bone mineral density in scoliosis by using quantitative computed tomography. Pol J
629 Radiol. 2019;84:e131-e5.
630 67. Wang Z, Chen H, Yu YE, Zhang J, Cheuk KY, Ng BK, et al. Unique local bone tissue
631 characteristics in iliac crest bone biopsy from adolescent idiopathic scoliosis with severe spinal
632 deformity. Sci Rep. 2017;7:40265.
633 68. Modi A, Piziak V. MON-355 Charge Syndrome: Unusual Cause of Hypogonadism
634 Leading to Osteoporosis. J Endocr Soc. 2020;4(Suppl 1):MON-355.
635 69. Kaneko T, Freeha K, Wu X, Mogi M, Uji S, Yokoi H, et al. Role of notochord cells and
636 sclerotome-derived cells in vertebral column development in fugu, Takifugu rubripes:
637 histological and gene expression analyses. Cell Tissue Res. 2016;366(1):37-49.
638 70. Jian QL, HuangFu WC, Lee YH, Liu IH. Age, but not short-term intensive swimming,
639 affects chondrocyte turnover in zebrafish vertebral cartilage. PeerJ. 2018;6:e5739.
640 71. Dale RM, Topczewski J. Identification of an evolutionarily conserved regulatory
641 element of the zebrafish col2a1a gene. Dev Biol. 2011;357(2):518-31.
642 72. Akiyama H, Chaboissier MC, Martin JF, Schedl A, de Crombrugghe B. The transcription factor
643 Sox9 has essential roles in successive steps of the chondrocyte differentiation pathway and is required
644 for expression of Sox5 and Sox6. Genes Dev. 2002;16(21):2813-28.
645 73. Bajpai R, Chen DA, Rada-Iglesias A, Zhang J, Xiong Y, Helms J, et al. CHD7 cooperates with PBAF
646 to control multipotent neural crest formation. Nature. 2010;463(7283):958-62.
647 74. Eames BF, Amores A, Yan YL, Postlethwait JH. Evolution of the osteoblast: skeletogenesis in gar
648 and zebrafish. BMC Evol Biol. 2012;12:27.
649 75. Hall AC. The Role of Chondrocyte Morphology and Volume in Controlling Phenotype-
650 Implications for Osteoarthritis, Cartilage Repair, and Cartilage Engineering. Curr Rheumatol Rep.
651 2019;21(8):38.
652 76. Lian C, Wang X, Qiu X, Wu Z, Gao B, Liu L, et al. Collagen type II suppresses articular chondrocyte
653 hypertrophy and osteoarthritis progression by promoting integrin beta1-SMAD1 interaction. Bone Res.
654 2019;7:8.
655 77. Westerfield M. The zebrafish book : a guide for the laboratory use of zebrafish (Danio rerio)
656 4th ed. [Text.]. Eugene, OR: Institute of Neuroscience, University of Oregon ,; 2000 [Available from:
657 http://zfish.uoregon.edu/zf_info/zfbook/zfbk.html.
658 78. Kimmel CB, Ballard WW, Kimmel SR, Ullmann B, Schilling TF. Stages of embryonic development
659 of the zebrafish. Dev Dyn. 1995;203(3):253-310.
660 79. Aceto J, Nourizadeh-Lillabadi R, Maree R, Dardenne N, Jeanray N, Wehenkel L, et al. Zebrafish
661 Bone and General Physiology Are Differently Affected by Hormones or Changes in Gravity. PLoS One.
662 2015;10(6):e0126928.
663 80. Otsu N. A Threshold Selection Method from Gray-Level Histograms. IEEE Transactions on
664 Systems, Man, and Cybernetics. 1979;9(1):62-6.

665

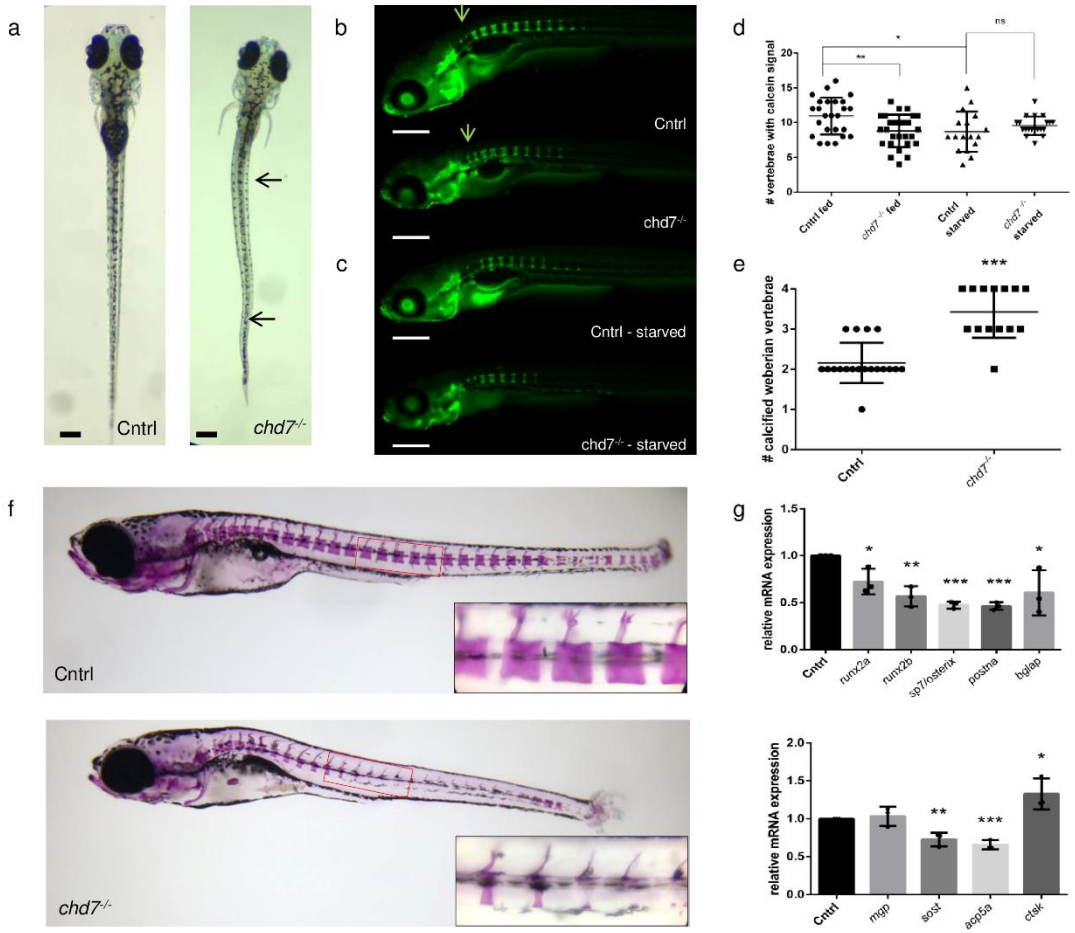

Fig 1. Mineralization in larval and juvenile *chd7*$^{-/-}$ mutants

a. Dorsal view of control and *chd7*$^{-/-}$ larvae at 9dpf showing severe spinal deformities in 43 out of 110 larvae screened. Deformities were present at both precaudal and caudal region (arrows). b. Lateral view of calcein staining at 9dpf showing mineralization of vertebrae with access to food starting at 5dpf and c. calcein staining at 9dpf during starvation. Arrow indicates mineralization at the first 4 (Weberian) vertebrae d. Number of vertebrae in wildtype and *chd7*$^{-/-}$ (fed and starved) larvae showing at least partial calcification signal as tested by calcein and e. Number of weberian vertebrae (vertebrae 1-4) showing complete calcification (see arrows in b) f. Lateral view of 4 week old zebrafish stained with alizarin red to screen mineralized vertebrae, showing decreased calcification towards posterior region. Bottom right corners show magnification of selected caudal vertebrae. g. RT-qPCR of osteogenesis related genes screened at 9dpf, showing relative fold change. (Significance: *p<0.05; **p<0.01)

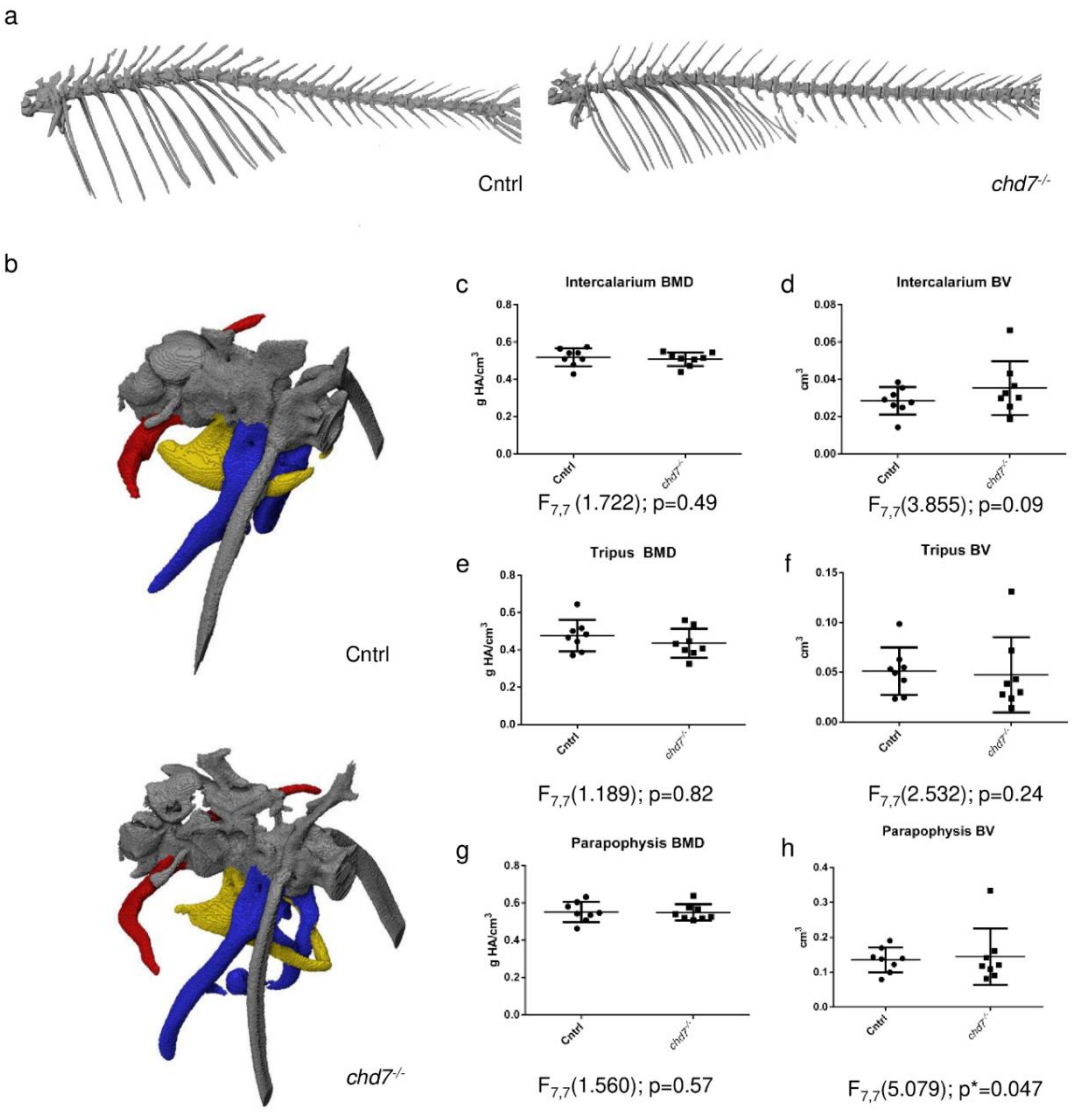

Fig 2. Weberian apparatus

a. Representative microCT overview image of the spinal cord from a 1-year old control and a *chd7*$^{-/-}$ adult zebrafish b. MicroCT Image of the Weberian apparatus from a 1-year old control and a *chd7*$^{-/-}$ mutants, indicating structures of intercalarium (red), tripus (yellow) and parapophysis (blue). c-h. vBMD and BV/TV of intercalarium (c, d) tripus (e, f) and parapophysis (g, h) (n=8/genotype were analyzed). Significance of student t-test with Welch's correction is included in the graphs with: *p<0.05; **p<0.01. F-test results are indicated underneath as $F_{\text{degree of freedom numerator, degree of freedom denominator}}$ (F-value); p-value: *p<0.05; **p<0.01; ***p<0.001

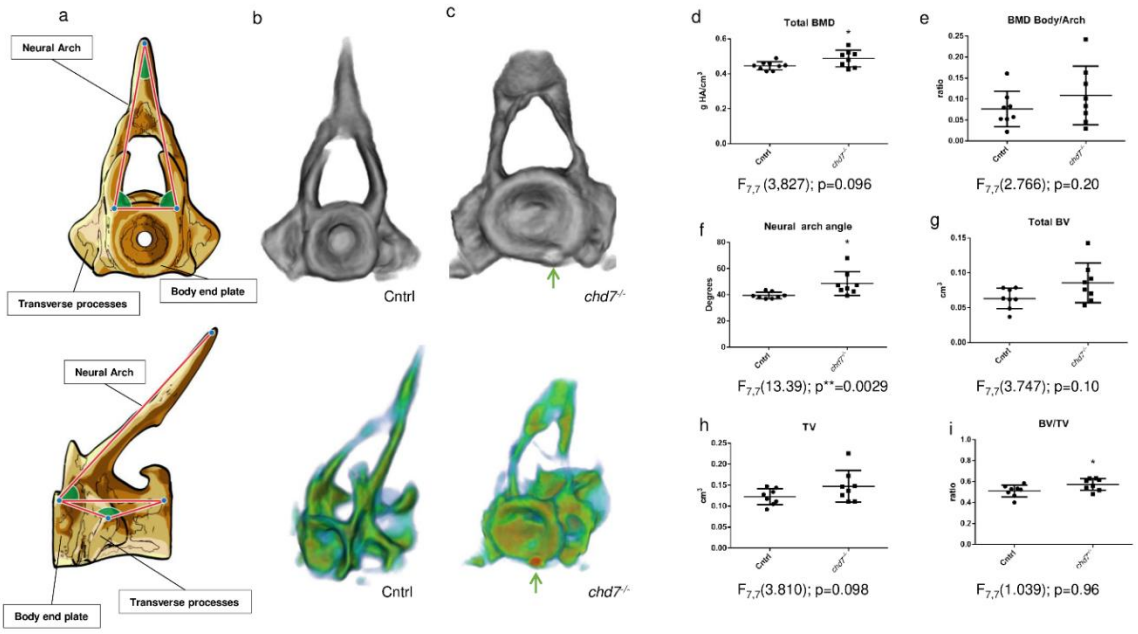

687

688 Fig 3. Precaudal vertebrae show inefficiency for proper mineralization

689 a. Sketch diagram of precaudal vertebrae (frontal and lateral) indicating structure and measured angles.
690 b-c. (top) Individual rendering of precaudal vertebrae, frontal view of tissue over 0.41 g HA/cm^3
691 threshold and (bottom) vBMD intensity map (Range blue-red; 0.41 – 1.00 g HA/cm^3) showing
692 morphological abnormalities and growth zone malformations with highly mineralized inclusions
693 (arrow) d. vBMD of whole vertebrae showing increasing density with increasing age and e. increasing
694 ratio of vBMD arch/vertebrae body. f-h neural arch angle, BV, TV and ratio BV/TV. (n=8/genotype
695 were analyzed). Significance of student t-test with Welch's correction is included in the graphs with:
696 *p<0.05; **p<0.01. F-test results are indicated underneath as $F_{\text{degree of freedom numerator, degree of freedom denominator}}$
697 (F-value); p-value: *p<0.05; **p<0.01; ***p<0.001

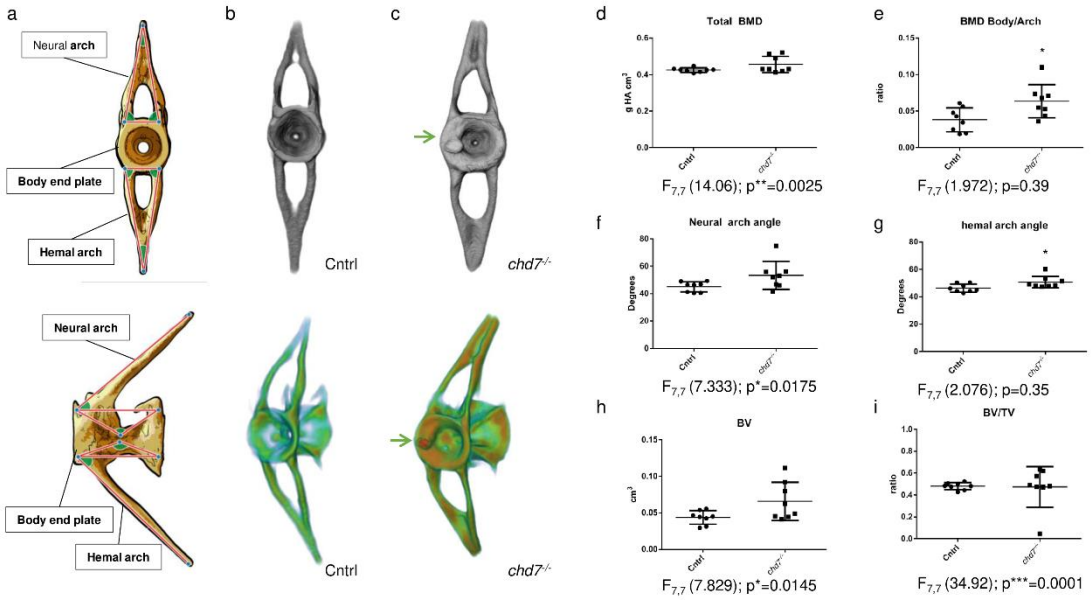

Fig 4. Caudal vertebrae show abnormal structure

a. Sketch diagram of precaudal vertebrae indicating structure and measured angles (frontal and lateral). b-c. (top) Individual rendering of caudal vertebrae, frontal view of tissue over 0.41 g HA/cm^3 threshold and (bottom) vBMD intensity map (Range blue-red; 0.41 – 1.00 g HA/cm3) showing morphological abnormalities and growth zone malformations with highly mineralized inclusions (arrow) d. vBMD of whole vertebrae and E. increasing ratio of vBMD arch/vertebrae body. f-h neural arch angle, BV, TV and ratio BV/TV. (n=8/genotype were analyzed). Significance of student t-test with Welch's correction is included in the graphs with: *p<0.05; **p<0.01. F-test results are indicated underneath as $F_{\text{degree of freedom numerator, degree of freedom denominator}}$ (F-value); p-value: *p<0.05; **p<0.01; ***p<0.001

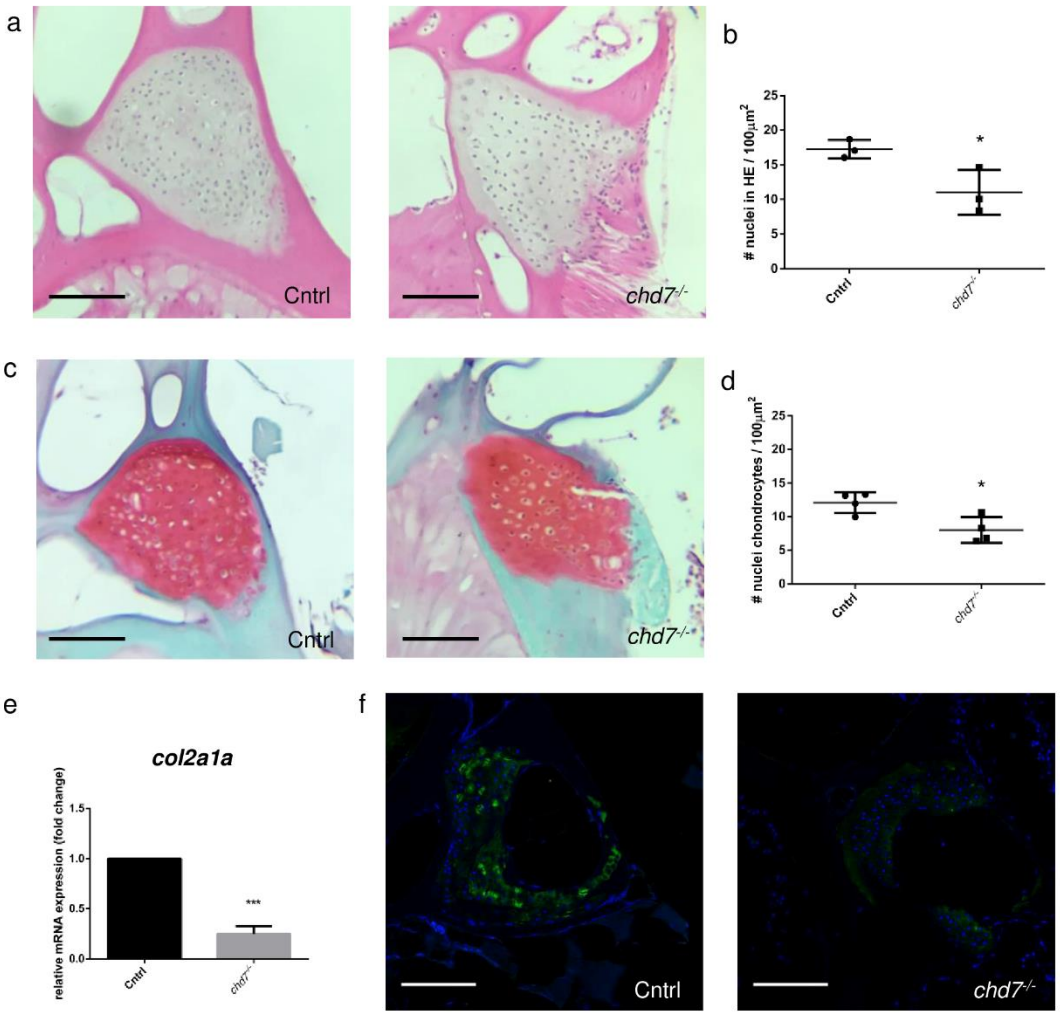

Fig 5. ECM Collagen deficiency in 1-year-old *chd7*$^{-/-}$ adults

a. H&E staining of precaudal vertebrae section of Cntrl and *chd7*$^{-/-}$ mutants b. Total nuclei count in precaudal vertebral cartilage detected in H&E staining per 100µm^2 c. Safranin O/fast green staining of precaudal vertebrae section Cntrl and *chd7*$^{-/-}$ mutants showing cartilage in red. d. Chondrocyte nuclei count in precaudal vertebral cartilage detected in Safranin O/fast green staining per 100µm^2 e. qPCR of *col2a1a* at 9dpf. f. Immunofluorescence of Col2a1 in precaudal vertebrae sections of Cntrl and *chd7*$^{-/-}$ mutants with Col2a1 in green and DAPI in blue. Scale bar presents 100µm. Significance of student t-test with: *p<0.05; **p<0.01 ***p<0.001